Highlights

A Virtual Mechanical System control law for energy transfer towards a single actuation point in n DOF buildings

Jasper Juchem, Sarah Geyskens, Kevin Dekemele, Mia Loccufier

- A virtual mechanical system (VMS) is attached to a vibrating structure via one actuator.
- The unique coupling between structure and VMS triggers a beating phenomenon.
- The unwanted energy is attracted and dissipated efficiently in the VMS.
- The VMS outperforms the passive state of the art controllers.

A Virtual Mechanical System control law for energy transfer towards a single actuation point in n DOF buildings

Jasper Juchem[a,1], Sarah Geyskens[a,1], Kevin Dekemele[a], Mia Loccufier[a]

[a] *Dept. Electromechanical, Systems and Metal Engineering, Ghent University, Technologiepark 125, Zwijnaarde, 9052, Belgium*

Abstract

Mitigating vibrations in engineering structures is of key interest, as they can lead to failure and/or discomfort. However, in some cases it is not feasible to actuate all the structure's degrees of freedom, which makes vibration mitigation difficult. In this work, we investigate the addition of a single one-degree-of-freedom virtual mechanical system (VMS), as an active controller, to attract and mitigate the energy from an impulse load on the structure. To challenge the controller, an actuation point is chosen furthest away from the impact location. As it is implemented virtually, the coupling between the structure and VMS can be chosen freely. It is found that a skew-symmetric coupling generates a gyroscopic force that enables control over the structure's mode shapes. Using this, the controller is tuned to achieve a beating phenomenon that attracts the vibration energy to the actuation location. A nonlinear damper, based on the slope of the envelope of the virtual velocity state, avoids reflection of energy to the structure and dissipates this unwanted energy. Furthermore, the virtual damper's robustness to timing errors is investigated: damping too soon means an incomplete energy transfer to the VMS, damping too late leads to return of energy to the building. The tuning strategy of the VMS is applied to a 4 DOF and 60 DOF building benchmark. For comparison, a tuned mass damper (TMD) and a nonlinear energy sink (NES) are tuned as well. The VMS succeeds in decreasing the settling time significantly in both cases, while the performance of the passive TMD and NES is rather limited for this specific configuration.

Keywords: energy transfer, vibration control, active control, high-rise building, underactuated control

1. Introduction

Buildings are prone to vibrations due to ground displacements, such as earthquakes and landslides or due to forces acting on the floors of a building, such as vibrating machinery present in the building and wind loads [1, 2, 3]. These vibrations lead to accelerations and deformations which can cause structural damage or discomfort for the building's residents [4, 5]. To study the effect of vibrations on a structure, two types of excitation are common: first, a periodic load, consisting of a single frequency or a limited number of frequencies, and, second, an impulse shock, which excites multiple natural frequencies. The former is perceived as an issue if a resonance frequency of the structure is approached. The latter triggers a number of natural frequencies simultaneously, thus, demanding a higher bandwidth in the used controllers.

Mitigating the vibrations in the structure is primordial to avoid its harmful effects. A first methodology is to modify the structure such that the (anti-)resonances are shifted to more feasible frequencies [6, 7, 8]. However, its capabilities are rather limited due to design, space and material restrictions. Part of it can be solved by creating a virtual structural modification using (semi-)active control [9, 10]. A second solution is to use passive vibration absorbers [11, 12]. A passive structure is added to match the eigenfrequency of the main structure, such that the energy is transferred to and dissipated in this additional structure. The disadvantage is that it can only be tuned to one specific frequency and two new resonances are created. The Nonlinear Energy Sink (NES) uses the nonlinearities (e.g. cubic springs) to circumvent this limitation and is able to capture multiple frequencies. Its robustness to initial energy is however rather limited. Also, the construction of nonlinear passive components can be tedious, even for simple nonlinear characteristics. A way to circumvent the latter is to use semi-active vibration absorbers [13, 14], the relative position, velocity and/or acceleration of the main system and vibration absorber are fed back to alter the stiffness and damping properties of the vibration absorber in real-time. The biggest advantage of passive and semi-active absorbers is that they do not affect the stability of the controlled systems. Hybrid vibration absorbers use

Email addresses: Jasper.Juchem@UGent.be (Jasper Juchem), Sarah.Geyskens@UGent.be (Sarah Geyskens)

[1]These authors contributed equally to this work.

an actuator to execute a control law in parallel with a passive device. They are able to mimic passive configurations beyond the restrictions of a physical realisation [15, 16].

An active controller uses information about the state of the main system that is fed to a control law. An actuator then exerts an action on the structure as dictated by the controller. The freedom granted by active control, due to the programmatic introduction of any complex control law, allows for an increased flexibility over the passive case [17]. This often leads to rather mathematical controllers, that are difficult to tune intuitively. Also, because energy is added to the system, via the actuator, it is important to take stability into consideration. An major drawback for (semi-)active and hybrid controllers is that they consume energy.

Interfering with the building's displacement is necessary, but it is not always feasible to interface with the structure on an arbitrary location. Due to design considerations, the most optimal location to damp vibrations might not be available for actuation. Therefore, it is useful to research underactuated control, where the number of controlled coordinates is less than the total amount of degrees of freedom (DOF). This is also beneficial to the complexity of implementation: more active control loops require more expensive sensors and actuators, more energy, and more complex controller design.

In this work, the aforementioned problems are tackled using an active control law that is inspired by the passive vibration absorber technology, as the tuning of these controllers is well understood. The displacement of a building's floor is read by a computer and is used to excite a virtual mechanical system (VMS). The generalised coordinates of the VMS are then used to exert a force on said floor. The added value compared to the passive solutions is that the coupling between the building and the additional VMS should not depend on the relative movement between both structures, but can be chosen arbitrarily. This gives the advantage over passive and semi-active vibration absorbers that the controller should not be placed at the location with the highest displacement, which is often the top floor. Moreover, it allows to implement an absorber of any complexity with any nonlinear component [18]. The goal is to transfer the energy as fast as possible, using the beating phenomenon, to the VMS, where nonlinear damping is used to dissipate the unwanted energy. No nonlinear stiffnesses are introduced, which avoids the creation of bifurcations. This allows to rely on linear tools.

To check its capabilities, the most challenging scenario is researched: a shock load is applied to the top floor and only the first floor can be measured and controlled. In Section 2 the methodology for a n DOF building is explained. First, the virtual mechanical structure is introduced, next the stability, based on Lyapunov's direct method, is proven, and finally, a tuning strategy based on the modal decomposition of the building is explained. In Section 3 and 4 the methodology of Section 2 is applied to a 4 DOF and 60 DOF building respectively. For each benchmark, a comparison is made with two passive vibration control devices, the Tuned Mass Damper (TMD) and Nonlinear Energy Sink (NES). These devices consist of a mass connected to the structure through a damper and (non)linear spring. In Section 5 the results and the methodology are discussed. And finally, the conclusions are formulated in Section 6.

2. Methodology

This paper investigates vibration mitigation in building structures. The model that is considered is depicted in Figure 1. The force that causes the vibrations is represented by an impulse on the n^{th} DOF, while the controller only works on the first DOF. This is the most challenging case as these locations are the furthest apart. For this reason, the focus lies on the energy transfer from the structure to the VMS, where it can be dissipated.

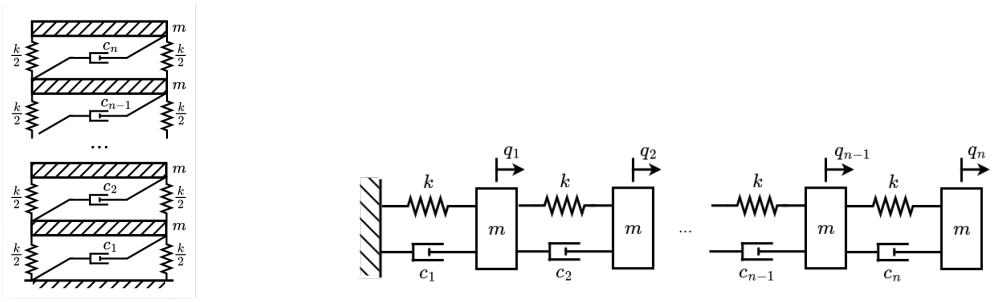

(a) (b)

Figure 1: (a) Lumped mass building model; (b) Equivalent mass-spring-damper model

2.1. Virtual mechanical system

An active controller is proposed which acts on the system through an actuator. The force exerted by the controller is computed by evaluating the dynamics of a virtual mechanical system (VMS). As it is an active controller, the only limitations on the control policy are imposed by the actuator and the control effort. There are no restrictions on the shape of the control signal, in contrast to the passive case. The dynamics of the controlled structure are described by

$$M\ddot{\mathbf{q}} + C\dot{\mathbf{q}} + K\mathbf{q} = F_{ext} + F_c, \tag{1}$$

where $M > 0$, $C > 0$ and $K > 0 \in \mathbb{R}^{n_p \times n_p}$ are respectively the inertia, damping and stiffness matrix of the building structure, $\mathbf{q} \in \mathbb{R}^{n_p}$ are the generalised coordinates, $F_{ext} \in \mathbb{R}^{n_p}$ is the external force causing the vibrations

$$F_{ext} = \begin{bmatrix} 0 & 0 & \cdots & 0 & \delta \end{bmatrix}^T \tag{2}$$

and $F_c \in \mathbb{R}^{n_p}$ is the force imposed by the controller with

$$F_c = \begin{bmatrix} f_{c1} & 0 & \cdots & 0 & 0 \end{bmatrix}^T. \tag{3}$$

The freedom obtained by the use of active control, allows us to choose the force by the controller F_c proportional to the velocity of a VMS. After all, forces that are proportional to velocity can have an effect on the damping and on the mode shapes of the system, according to [19]. The dynamics of the combined system can be expressed as

$$\begin{cases} M\ddot{\mathbf{q}} + C\dot{\mathbf{q}} + K\mathbf{q} = F_{ext} - \nu\dot{\mathbf{z}} \\ D_0\ddot{\mathbf{z}} + \frac{\partial \mathbf{F}}{\partial \dot{\mathbf{z}}}(\dot{\mathbf{z}}) + K_0\mathbf{z} = -N\dot{\mathbf{q}} \end{cases}, \tag{4}$$

where $\mathbf{z} \in \mathbb{R}^{n_c}$ are the generalised coordinates of the VMS, the coupling terms $\nu \in \mathbb{R}^{n_p \times n_c}$ and $N \in \mathbb{R}^{n_c \times n_p}$, can be expressed as

$$\nu = \begin{bmatrix} \nu_1 & \nu_2 & \cdots & \nu_{n_c} \\ 0 & 0 & \cdots & 0 \\ \vdots & \vdots & \ddots & \vdots \\ 0 & 0 & \cdots & 0 \end{bmatrix} \qquad N = \begin{bmatrix} N_1 & 0 & \cdots & 0 \\ N_2 & 0 & \cdots & 0 \\ \vdots & \vdots & \ddots & \vdots \\ N_{n_c} & 0 & \cdots & 0 \end{bmatrix}, \tag{5}$$

and $D_0 > 0 \in \mathbb{R}^{n_c \times n_c}$, $\frac{\partial \mathbf{F}}{\partial \dot{\mathbf{z}}}(\dot{\mathbf{z}}) \in \mathbb{R}^{n_c}$ and $K_0 > 0 \in \mathbb{R}^{n_c \times n_c}$ are respectively the inertia, damping term and stiffness of the VMS.

2.1.1. Stability

To prove stability, Lyapunov's direct method is used. A straightforward Lyapunov candidate is the Hamiltonian. Due to the coupling, the Hamiltonian needs to be carefully defined. After all, the coupling can contribute to conservative forces, and should thus be included in the expression of the kinetic and/or potential energy of (4).

System (4) can be written in matrix form:

$$\begin{bmatrix} M & 0 \\ 0 & D_0 \end{bmatrix} \dot{\mathbf{v}} + \begin{bmatrix} C\dot{\mathbf{q}} \\ \frac{\partial \mathbf{F}}{\partial \dot{\mathbf{z}}}(\dot{\mathbf{z}}) \end{bmatrix} + \underbrace{\begin{bmatrix} 0 & \nu \\ N & 0 \end{bmatrix}}_{R} \dot{\mathbf{v}} + \begin{bmatrix} K & 0 \\ 0 & K_0 \end{bmatrix} \mathbf{v} = \begin{bmatrix} F_{ext} \\ 0 \end{bmatrix} \tag{6}$$

with $\mathbf{v} = [\mathbf{q}^T, \mathbf{z}^T]^T$. The second term are the non-conservative damping terms. At this point, it is not clear if matrix R contains (non-)conservative forces. In [19] it is proposed to separate the symmetric and skew-symmetric parts of the velocity- and position-dependent terms. The symmetric (S) and skew-symmetric (SS) part are given by

$$R^S = \frac{1}{2}(R + R^T) = \frac{1}{2}\begin{bmatrix} 0 & \nu + N^T \\ \nu^T + N & 0 \end{bmatrix}, \tag{7}$$

$$R^{SS} = \frac{1}{2}(R - R^T) = \frac{1}{2}\begin{bmatrix} 0 & \nu - N^T \\ N - \nu^T & 0 \end{bmatrix}. \tag{8}$$

The hypothesis is that the skew-symmetric part will contribute to the conservative forces and should thus be included in the kinetic energy. The kinetic energy can be found from the inverse Euler-Lagrange formalism:

$$\begin{cases} \frac{d}{dt}\frac{\partial T_R}{\partial \dot{\mathbf{q}}} = \frac{1}{2}(\nu - N^T)\dot{\mathbf{z}} \\ \frac{d}{dt}\frac{\partial T_R}{\partial \dot{\mathbf{z}}} = \frac{1}{2}(N - \nu^T)\dot{\mathbf{q}} \end{cases} \tag{9}$$

The kinetic energy T of the controlled system then becomes

$$T = \frac{1}{2}\dot{\mathbf{q}}^T M \dot{\mathbf{q}} + \frac{1}{2}\dot{\mathbf{z}}^T D_0 \dot{\mathbf{z}} + \frac{1}{2}\dot{\mathbf{q}}^T(\nu - N^T)\mathbf{z} + \frac{1}{2}\mathbf{q}^T(N^T - \nu)\dot{\mathbf{z}}. \tag{10}$$

The Hamiltonian is given by

$$\mathcal{H} = \sum_{\alpha = \mathbf{q},\mathbf{z}} p_\alpha \dot{\alpha} - \mathcal{L} \tag{11}$$

with $\mathcal{L} = T - V$ the Lagrangian, V the potential energy, $p_\alpha = \frac{\partial T}{\partial \dot{\alpha}}$ the generalised momenta. This results in

$$\mathcal{H} = \frac{1}{2}\dot{\mathbf{q}}^T M \dot{\mathbf{q}} + \frac{1}{2}\dot{\mathbf{z}} D_0 \dot{\mathbf{z}} + V \tag{12}$$

Notice that the coupling does not contribute to the Hamiltonian.

For Lyapunov's direct method, global asymptotic stability is guaranteed if the following is fulfilled:

1. the Lyapunov candidate and its gradient is continuous,
2. the Lyapunov candidate reaches a minimum in the equilibrium point,
3. the time derivative of the Lyapunov candidate along the solutions of the system is smaller than zero, except for the equilibrium point.

The first condition is trivially satisfied. The second condition is examined using the Hessian. First, it is noticed that $\mathcal{H} \geq V$, so it is sufficient to examine the potential energy. The Hessian of the potential energy function is given by

$$\mathcal{H}_f = \begin{bmatrix} K & 0 \\ 0 & K_0 \end{bmatrix}. \tag{13}$$

A minimum is reached if $\mathcal{H}_f > 0$. The matrix is block diagonal, so $K, K_0 > 0$ should be satisfied. Hence, condition 2 is satisfied. The third condition results in

$$\frac{d\mathcal{H}}{dt} = -\dot{\mathbf{z}}^T(\nu^T + N)\dot{\mathbf{q}} - \dot{\mathbf{q}}^T C \dot{\mathbf{q}} - \frac{\partial \mathbf{F}}{\partial \dot{\mathbf{z}}}(\dot{\mathbf{z}})^T \dot{\mathbf{z}}. \tag{14}$$

As $C > 0$, the second term is always smaller or equal to 0. The other two terms depend on the tuning of the controller. The first term is not trivially smaller or equal to 0, but can be omitted by choosing

$$N = -\nu^T. \tag{15}$$

Notice, that $R^S \equiv 0$ in this case. This accords with the finding in [19] that the symmetric part contributes to a non-conservative force. Now, $\frac{\partial \mathbf{F}}{\partial \dot{\mathbf{z}}}(\dot{\mathbf{z}})^T \dot{\mathbf{z}} > 0$ if $\dot{\mathbf{z}} \neq 0$ needs to be satisfied. This leads to global asymptotical stability.

2.1.2. Single degree of freedom controllers

The main research questions in this work is whether the active VMS controller, with its unique coupling, can be advantageous in attracting and mitigating vibrations, using a

single actuation point. To evaluate its performance it is compared to the passive state-of-the-art: tuned mass dampers (TMDs) and nonlinear energy sinks (NESs). Up until now, we have generalised the controller to have dimension $n_c \in \mathbb{N}_0$. However, to show and analyse the performance of the VMS controller it is sufficient to simplify the controllers' dimension to one from now on. This will allow to capture the most dominant behaviour of the system, hence, showing its working principle clearly. Furthermore, the passive solutions often resort to adding systems with one degree of freedom. Therefore, it is appropriate to compare a VMS controller with $n_c = 1$ with a passive controller with one generalised coordinate. Based on this, the controller's dimension is from now on $n_c = 1$, unless stated otherwise.

2.1.3. Tuning

In this section, the focus lies on creating a heuristic to tune the controller parameters to facilitate energy transfer to the VMS. Without loss of generality, the inertia of the controller D_0 can be set equal to one. The damping term in the controller is not yet considered.

Under the condition that the behaviour of the structure, subjected to an impulse load, can be approximated by a limited number of dominant modes, a modal decomposition can be conducted to gain insight in the dominant behaviour.

The eigenfrequencies ω_i and eigenvectors $\mathbf{e_i}$ of the undamped n DOF system are calculated such that

$$(K - \omega_i^2 M)\mathbf{e_i} = \mathbf{0}, \tag{16}$$

where $\omega_1 < \omega_2 < ... < \omega_n$. With these eigenvectors, which have been mass-normalised, the modal matrix E is formed:

$$E = \begin{bmatrix} \mathbf{e_1} & \mathbf{e_2} & ... & \mathbf{e_{n_c}} \end{bmatrix}. \tag{17}$$

The modal decomposition is achieved using the coordinate transformation $\mathbf{q} = E\mathbf{p}$. The system model in modal coordinates $\mathbf{p}$, premultiplied with E^T becomes

$$E^T M E\ddot{\mathbf{p}} + E^T C E\dot{\mathbf{p}} + E^T K E\mathbf{p} = E^T N^T \dot{\mathbf{z}} + E^T F_{ext} \tag{18}$$

$$\iff I\ddot{\mathbf{p}} + C_p\dot{\mathbf{p}} + diag(\omega_i^2)\mathbf{p} = E^T N^T \dot{\mathbf{z}} + E^T F_{ext} \tag{19}$$

with C_p a diagonal matrix in this work.

The dynamics of the dominant mode p_1, corresponding to eigenfrequency ω_1, are extracted, while assuming the other modes are present to a lesser extent and can be neglected. This results in

$$\ddot{p}_1 + c_p\dot{p}_1 + \omega_1^2 p_1 = \alpha N_1 \dot{z} + \beta\delta, \tag{20}$$

where $c_p = C_p[1,1]$, $\alpha = E[1,1]$, $\beta = E[n_p, 1]$. Notice that the number of dominant modes that are being considered, determines the dimension of the controller. The controller model in modal coordinates is

$$\ddot{z} + K_0\mathbf{z} = -\alpha N_1 \dot{p}_1 \tag{21}$$

Where, once again, the approximation is only valid when p_1 is the dominant mode of the original system. Finally, the equations describing the approximated system in matrix form are

$$\begin{bmatrix} \ddot{p}_1 \\ \ddot{z} \end{bmatrix} + \begin{bmatrix} c_p & -\alpha N_1 \\ \alpha N_1 & 0 \end{bmatrix} \begin{bmatrix} \dot{p}_1 \\ \dot{z} \end{bmatrix} + \begin{bmatrix} \omega_1^2 & 0 \\ 0 & K_0 \end{bmatrix} \begin{bmatrix} p_1 \\ z \end{bmatrix} = \begin{bmatrix} \beta\delta \\ 0 \end{bmatrix}. \tag{22}$$

This simplified system encompasses the dominant behaviour of combined system, consisting of the n_p DOF structure and the 1 DOF controller. Its characteristic equation is investigated to gain insight in the controller parameters

$$\det\left(\begin{bmatrix} \lambda^2 + c_p\lambda + \omega_1^2 & -\alpha N_1 \lambda \\ \alpha N_1 \lambda & \lambda^2 + K_0 \end{bmatrix}\right) = 0 \tag{23}$$

Specific choices of K_0 and N_1 allow the poles of (20) and (21) to coincide. If the controller parameters are chosen as

$$K_0 = \omega_1^2, \tag{24}$$

$$N_1 = \pm\frac{c_p}{2\alpha}, \tag{25}$$

the characteristic equation (23) reduces to

$$(\lambda^2 + \frac{c_p}{2}\lambda + \omega_1^2)^2 = 0. \tag{26}$$

For the original combined system this cannot be guaranteed due to the influence of other modes. However, this choice for the parameters does ensure that the dominant pole with frequency f_p lies close to the pole, with frequency f_c, of the controller.

These poles cause a beating phenomenon to occur, which allows energy to transfer from the structure to the controller. The beating frequency of the dominant mode is given by

$$f_{beat} = \frac{|f_p - f_c|}{2}, \tag{27}$$

which means that shifting the poles closer together implies a slower energy transfer, and separating the poles implies a higher beat frequency.

Depending on the requirements of a certain application, further optimisation of N_1 is possible, where expression (25) can offer a suitable initial value.

2.1.4. Damping

The objective of adding nonlinear damping to the controller, is to take advantage of the beating phenomenon. More specifically, once the energy has been attracted to the VMS, it must be dissipated. An important consideration in selecting the damping characteristic, is that energy transfer towards the VMS is favourable, while energy transfer in the other direction should be inhibited.

The ideal scenario is that no damping is present when energy is being attracted to the controller, so all energy can be transferred and then dissipated before it could return to the system. In simulations, this can be achieved with a switch that adds a large damping term once the values of the local maxima of the responses start decreasing. This is the moment that the energy starts flowing back to the structure. As an active controller is used, this can straightforwardly be calculated online.

Damping as a function of the envelope of $\dot{z}$, denoted as $\bar{\dot{z}}$, is proposed. Figure 2 is an example of such a characteristic. The hysteresis facilitates energy attraction to the controller while impeding the reverse path.

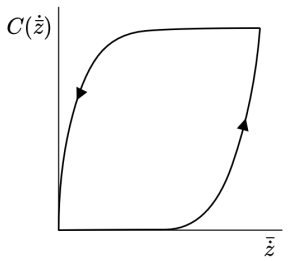

Figure 2: Possible damping characteristic

It should be noticed that the analysis of an appropriate and performant nonlinear damping function is a complex matter, and should be researched in detail. However, this is out of the scope of this work. An analysis on the robustness of the damping is done in the example of the 4 DOF building.

The next sections describe the implementation of the presented control method on a 4 DOF and 60 DOF building structure.

3. Example - 4 DOF building

Let us consider the case where an impulse load, that introduces vibrations, is applied at q_4, the generalised coordinate of the top floor, while the active controller is attached to q_1, the furthest from the energy source. This load is equivalent to setting an initial condition $\dot{q}_4$, chosen $1m/s$ here, while all other initial velocities are zero. First, the tuning methodology of Section 2.1.3 with the VMS will be applied to the 4 DOF building. Next, a TMD and NES will be tuned for this system, as they represent the state-of-the-art in (passive) vibration control of buildings.

The matrices of (1) read

$$M = \begin{bmatrix} m & 0 & 0 & 0 \\ 0 & m & 0 & 0 \\ 0 & 0 & m & 0 \\ 0 & 0 & 0 & m \end{bmatrix}, \; m = 5.706 \; [kg], \tag{28}$$

$$C = \begin{bmatrix} 7.079 & -2.039 & -0.365 & -0.177 \\ -2.039 & 6.713 & -2.216 & -0.542 \\ -0.365 & -2.216 & 6.536 & -2.581 \\ -0.177 & -0.542 & -2.581 & 4.497 \end{bmatrix} \left[N\frac{s}{m}\right], \tag{29}$$

$$K = \begin{bmatrix} 2k & -k & 0 & 0 \\ -k & 2k & -k & 0 \\ 0 & -k & 2k & -k \\ 0 & 0 & -k & k \end{bmatrix}, \; k = 11923 \; \left[\frac{N}{m}\right]. \tag{30}$$

Note that the damping matrix C corresponds to a damping ratio of 1%.

3.1. Virtual mechanical system

It can be observed from the impulse response that the system has one dominant mode, being the lowest frequency mode. The VMS is a one DOF system connected to the building at floor 1. The following model describes its dynamics:

$$\ddot{z} + \frac{\partial F}{\partial \dot{z}}(\dot{z}) + K_0 z = -\mathbf{N}\dot{\mathbf{q}}, \tag{31}$$

where $\mathbf{N} = \begin{bmatrix} N_1 & 0 & 0 & 0 \end{bmatrix}$. Notice that the mass is chosen to be $1kg$ without loss of generality, as mentioned before. The parameters that need to be tuned are $K_0 \in \mathbb{R}$, $N_1 \in \mathbb{R}$ and the damping term $\frac{\partial F}{\partial \dot{z}}(\dot{z})$. As described is Section 2.1.3, the VMS is first considered without damping ($\frac{\partial F}{\partial \dot{z}}(\dot{z}) \equiv 0$).

Virtual stiffness K_0 is chosen in order to match the undamped eigenfrequency of the VMS to the dominant frequency of the original system (see (24)). The frequency spectra show that the dominant frequency is the same for each DOF of the structure, namely $\omega_{dom} = 15.88$ rad/s, corresponding to mode 1. From which follows that $K_0 = \omega_{dom}^2 \cdot 1kg = 252.03\frac{N}{m}$.

3.2. Modal system approximation

In Figure 3 the root-loci of the controlled system's (18) poles are considered where N_1 is varied and $K_0 = \omega_1^2$. As expected, the branches corresponding to the dominant poles (closest to the imaginary axis) first approach and then diverge. The value of N_1 where the poles are the closest is estimated using the modal approximation.

The simplified model for the 4 DOF system and controller computed using the modal method according to Eq. (22) is

$$\begin{bmatrix} \ddot{p_1} \\ \ddot{z} \end{bmatrix} + \begin{bmatrix} c_p & -\alpha N_1 \\ \alpha N_1 & 0 \end{bmatrix} \begin{bmatrix} \dot{p} \\ \dot{z} \end{bmatrix} + \begin{bmatrix} \omega_1^2 & 0 \\ 0 & \omega_1^2 \end{bmatrix} \begin{bmatrix} p_1 \\ z \end{bmatrix} = \begin{bmatrix} \beta\delta \\ 0 \end{bmatrix}, \tag{32}$$

where $\omega_1 = 15.88$, $c_p = 0.33$, $\alpha = 0.046$ and $\beta = 0.30$.

To confirm that the simplified system returns a valid estimate for the dominant behaviour, its poles for varying N_1 are compared with to the original ones. This is depicted by the root-loci for N_1 in Figure 4, where the black dots represent the poles of the real controlled system (18), and the blue line shows the poles of the simplified controlled system (32), both in function of N_1. In contrast to the root-loci of the original

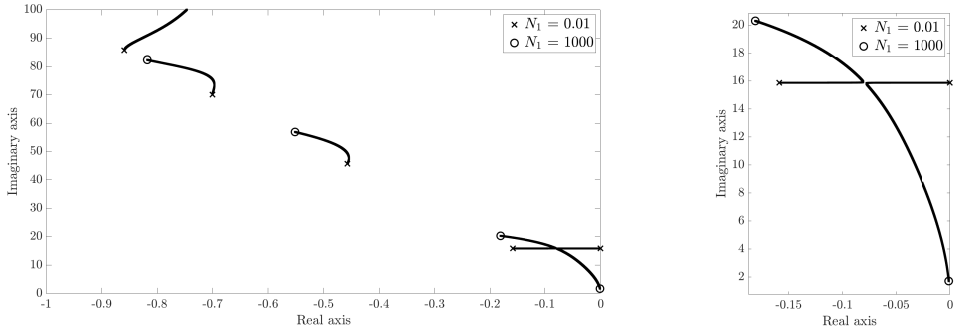

Figure 3: Evolution of poles with varying N_1 for the 4 DOF case; (a) Evolution of poles with varying N_1. (b) Close up.

system, those of the simplified system (blue) coincide for a certain $N_1 = 1.6635$, found with (25) (Fig. 4, blue cross). In the original controlled system, this specific value for N_1 corresponds to the situation that the two black root-loci are close to each other (Fig. 4, black crosses). This confirms that the simplified system is a good estimate of the actual system.

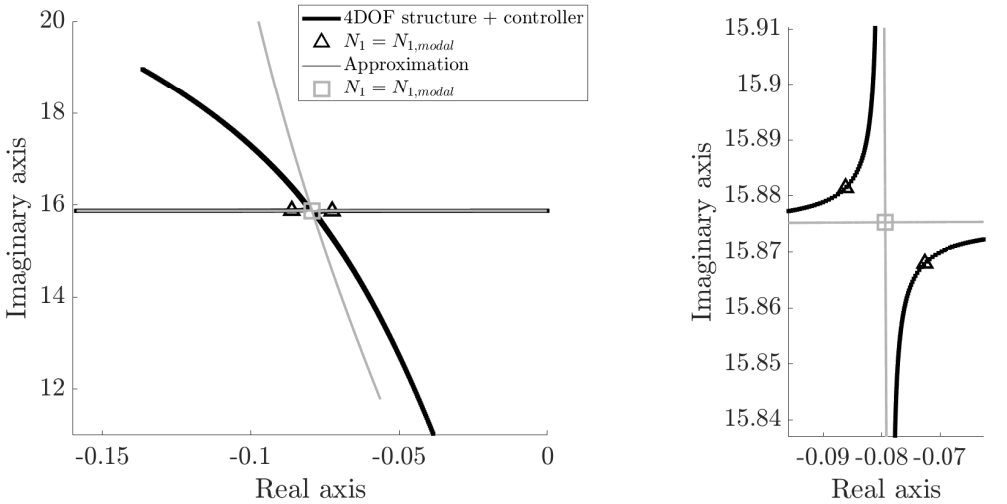

(a) Dominant poles for N_1 from 0.01 to 100

(b) Close up around $N_1 = 1.6635$

Figure 4: Comparison of dominant poles with varying N_1 for original system and simplification for the 4 DOF case study.

The impulse response of the generalised coordinate of the top floor q_4 for this N_1 can be found in Figure 5a. A similar plot can be obtained for the other floors. A beating phenomenon can be observed: the energy is transferred from all system coordinates q_i to the virtual coordinate z, and vice versa.

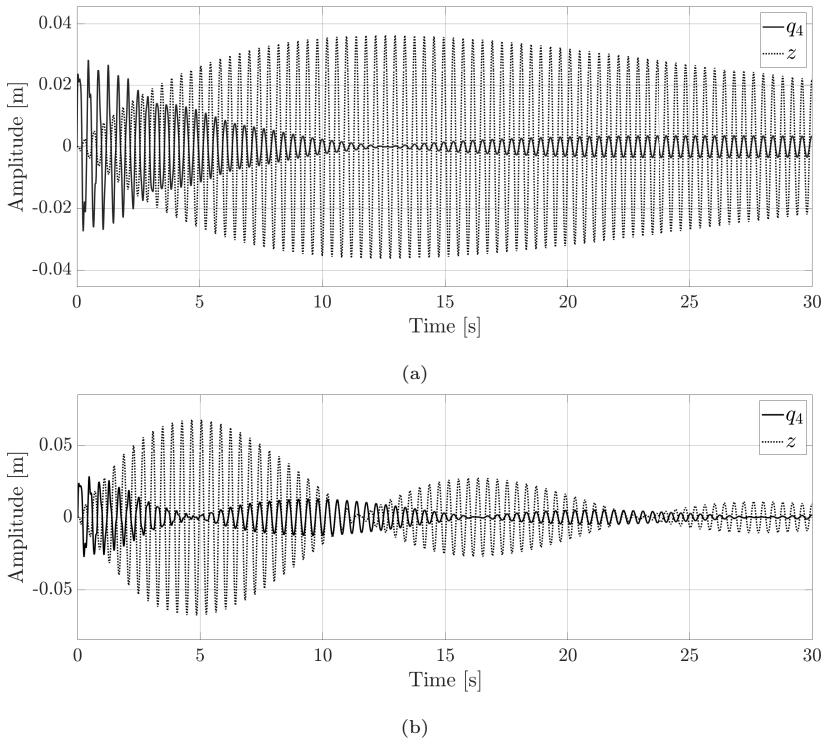

Figure 5: Impulse responses of the controlled system at q_4 without controller damping for the 4 DOF case; (a) $N_1 = 1.6635$ (b) $N_1 = 5.9467$.

From Figure 5a, one can observe that around $t = 12.5s$, approximately all energy has been transferred to the controller. This behaviour, if appropriate damping is added, can be exploited to bring all coordinates to a standstill as fast as possible.

In this work, the performance of the controller will be evaluated based on the 2%-settling time of each generalised coordinate. This is the amount of time during which the amplitude of a generalised coordinate's oscillation reduces with 98%. According to (27), a faster beating frequency and, thus, a faster settling time can be achieved by further separating the poles. Figure 6 demonstrates that increasing N_1 can increase the beating

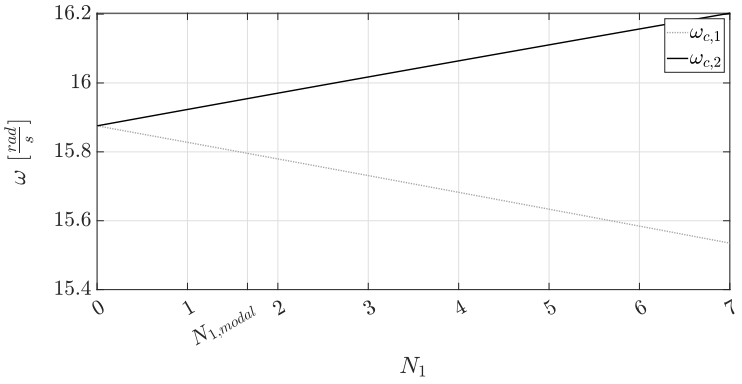

Figure 6: Eigenfrequencies of the dominant modes of the controlled 4 DOF system without damping in function of N_1.

frequency, which results in a higher rate of energy transfer. The two frequency branches of Figure 6 originating at ω_1 for $N_1 = 0$ is typical for a gyroscopic, mechanical system. This property is created due to the skew-symmetric coupling of the main systems and the controller. However, an optimal value for N_1 exists and, by optimising the settling times of the generalised coordinates of the structure, a value of 5.9467 is found. The time response for this case is depicted in Figure 5b. To understand the trade-off, we refer to Figure 5. When comparing the impulse responses of $N_1 = 1.6635$ (Figure 5a) and $N_1 = 5.9467$ (Figure 5b) it can be seen that in the latter the energy is transferred more quickly, but not completely, i.e. when the envelope of z is maximal, the amplitudes of $\mathbf{q}$ are not zero. This can result in the undesirable situation that more than one beat period is required to reach the 2% settling time.

3.3. Nonlinear damping

Subsequently, the ideal damping term is added to the simulations:

$$\frac{\partial F}{\partial \dot{z}}(\dot{z}) = C_z(\dot{z})\dot{z}, \tag{33}$$

where

$$C_z(\dot{z}) = \begin{cases} \epsilon, & t \leq t_{switch} \\ 10, & t > t_{switch} \end{cases} \tag{34}$$

Here, ϵ is a small positive real number to abide to the stability criteria, the value of the damping constant after t_{switch} is chosen to decrease the settling time of the virtual coordinate as fast as possible, t_{switch} is the instant at which the amplitude of a peak of $\dot{z}$ is lower than the previous one. This means the envelope of $\dot{z}$ is decreasing and the energy is starting to flow back to the structure. Notice that the damping function (34) is an oversimplified version of the damping function in Figure 2, however, the overall rationale is similar. This damping term complies with the stability conditions presented in Section 2.1.1. The evolution of the damping factor C_z and resulting behaviour of the combined system is presented in Figure 7a in the ideal case. However, in reality such an abrupt change in damping force is not feasible, as it would require the actuator to stop its inertia immediately. So, a less ideal, but more feasible solution is to ramp up the damping force gradually, which can be seen as introducing an actuator rate limit effect, as shown in Figure 2 [20]. The time derivative of the envelope of $\dot{z}$ is inversely proportional to the damping force, until the time derivative is zero and the damping reaches its maximum. This is achieved using a sigmoid-function and is shown in Figure 7b. The damping term is given by

$$C_z(\dot{z}) = \frac{10}{1 + \exp\left(-10(t - t_{switch})\right)} \tag{35}$$

There is a clear difference in the first period after the damping is activated. The amplitude of the virtual coordinate is higher for the sigmoid damping compared to the ideal case. For the remainder of the time signal the result is similar.

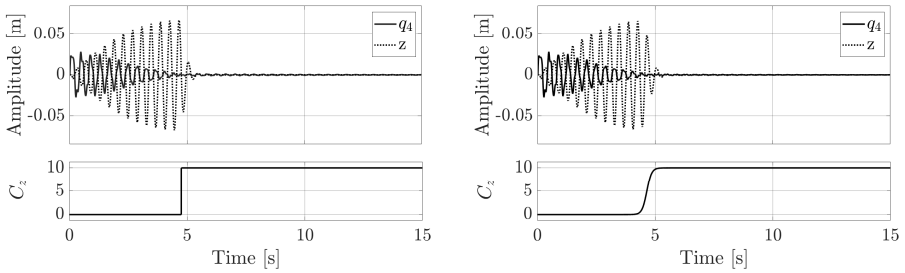

(a) (b)

Figure 7: Evolution of C_z and time response of damped combined system in (a) the ideal case, and (b) with a sigmoid damping function to mimic a more realistic damping force.

The quality of the damping force depends on the estimate of the envelope of $\dot{z}$. As the

damping force reaches its maximum too soon (see Figure 8a), the energy transfer from the building to the VMS is not complete yet, and energy remains in the building. If the damping force reaches its maximum too late (see Figure 8b), part of the energy will flow back to the building, increasing the settling time. But in both cases, the response is still acceptable. A further discussion on the quality of the estimate of the envelope can be found in Section 5. In this context, it can be remarked that the NES often has a residual energy remaining in the main system as well, as the activation threshold is crossed when the energy is removed from the main system. There, one relies on the internal damping of the main system to remove this residual energy. This is also the case for the early and late damping forces in Figures 8a and 8b respectively.

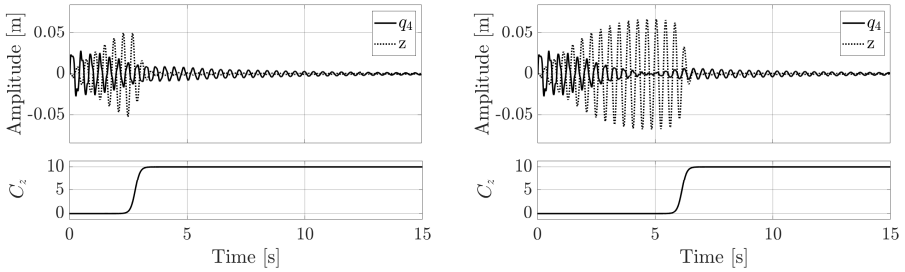

(a) (b)

Figure 8: Evolution of C_z and time response of damped combined system in (a) the ideal case, and (b) with a sigmoid damping function to mimic a more realistic damping force.

3.4. TMD/NES

Here, the tuning of the two passive control devices, TMD and NES, is explained. They represent the state-of-the-art in vibration control of buildings and have shown to be very performant. However, they have their drawbacks, which can be circumvented by using active control. One DOF passive controllers are considered, as they are common, and result in a fair comparison with the one DOF VMS controller.

The TMD consists of a mass, linear damping and a linear spring, while the NES has the same components except for a nonlinear spring. The TMD is tuned such that its own natural frequency is close to a natural frequency of the structure, and such that this natural frequency is critically damped, meaning that it is optimised for settling time

under transient loads [21, 22]:

$$\mu_i = m_{\mathrm{a}}\mathbf{e_i}(\ell)^2 \quad \omega_{\mathrm{a}}^2 = \frac{k_{\mathrm{a}}}{m_{\mathrm{a}}} = \frac{\omega_i^2}{1+\mu_i} \quad \zeta_a = \frac{c_{\mathrm{a}}}{2m_{\mathrm{a}}\omega_{\mathrm{a}}} = \sqrt{\frac{\mu_i}{1+\mu_i}} \tag{36}$$

where m_{a}, k_{a}, c_{a} are the TMD's mass, stiffness and damping, and $\mathbf{e_i}(\ell)$ the eigenvector component of mode i at the connection point of the TMD ℓ. Here, it is opted again to attach the TMD to the first floor, $\ell = 1$. Usually, a mass m_{a} is proposed, which is typically chosen as 0.5% of the total mass of the building, and, like for the VMS controller, the TMD's eigenfrequency is close to the most dominant eigenfrequency of the structure, which is the first mode. From this, the required k_{a} and c_{a} are determined. The numerical values for the components of the TMD can be found in Table 1.

Table 1: Parameters of the TMD/NES for the 4 DOF building.

$m_a[kg]$	$c_a[Ns/m]$	$k_a[N/m]$	$c_{na}[Ns/m]$	$k_{na}[N/m]$
0.1141	0.1167	28.7020	0.2265	$6.631 \cdot 10^4$

The NES is the state-of-the-art passive vibration absorber that is able to self-tune to the eigenfrequencies through its nonlinear spring. Usually, this spring is of a hardening polynomial kind, here x^3. When attached to an MDOF structure under impulse load, the NES engages in Resonance Capture Cascade (RCC) where it transfers and dissipates the several eigenfrequencies from high to low frequency [23] or from low to high frequency [24]. This is in contrast to the TMD which only targets one eigenfrequency. However, while the TMD has viscous damping, meaning that it damps vibrations exponentially, the NES will always leave a residual amount of vibration energy. To design the NES, the mass of the nonlinear absorber is here again chosen as 0.5% of the structure's mass. The NES' mass is attached to the first mass through a cubic polynomial stiffness ($k_{\mathrm{na}}(q_{\mathrm{na}} - q_1)^3$) and linear viscous damping ($c_{\mathrm{na}}(\dot{q}_{\mathrm{na}} - \dot{q}_1)$). The NES' stiffness and damping coefficients are chosen such that 10% of the energy remains of mode 1 for an impulse load at $\dot{q}_4 = 1\frac{m}{s}$. The parameters are tuned as follows

$$c_{\mathrm{a}} = 0.125 m_{\mathrm{a}}\omega_i \quad k_{\mathrm{na}} = 0.205\frac{m_{\mathrm{a}}\omega_i^4}{\mathbf{e_i}(\ell)^2\dot{p}_i(0)^2} \tag{37}$$

where $i = \ell = 1$ and $\dot{p}_i(0)$ is the initial modal speed of mode i. The numerical values can be found in Table 1. For more details on this tuning methodology, the reader is referred

to [25].

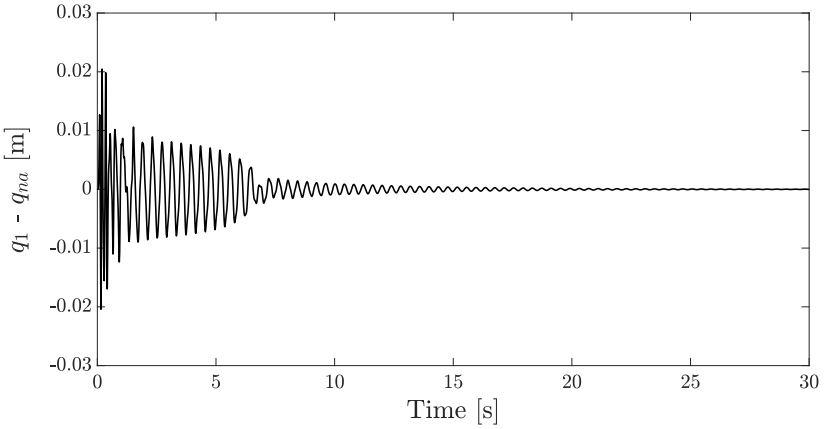

Figure 9: Time response of relative coordinate of NES

The RCC is clearly visible in Figure 9, which shows the time vector of the relative coordinate of the NES. The RCC is able to capture two vibration modes: during the first half second, the absorber vibrates with the second eigenfrequencies, and then from 0.5s to 6s with the first eigenfrequency. The envelopes of the time responses of q_4, the generalised coordinate with largest amplitude and furthest from the vibration absorbing systems, are plotted in Figure 10 for the different vibration control strategies. This simplified representation of the time signal allows to analyse the decay of the energy. It is clear that both the uncontrolled system and the structure with the TMD experience an exponential decay. The building with the NES and VMS do not have a purely exponential decay. Two different zones can be discerned: between 1s and 5s a faster decay is observed, after that a slower decay can be seen.

The 2%-settling times for each vibration mitigation strategy can be found in Table 2. Notice that the VMS controller is able to decrease the settling time significantly. The TMD and NES only show a small improvement compared to the VMS controller.

3.5. Robustness

The robustness of these vibration mitigation techniques is reviewed by investigating their capability to deal with model errors and differences in the magnitude of the load. The model errors are simulated by changing the eigenfrequency of the structure, more

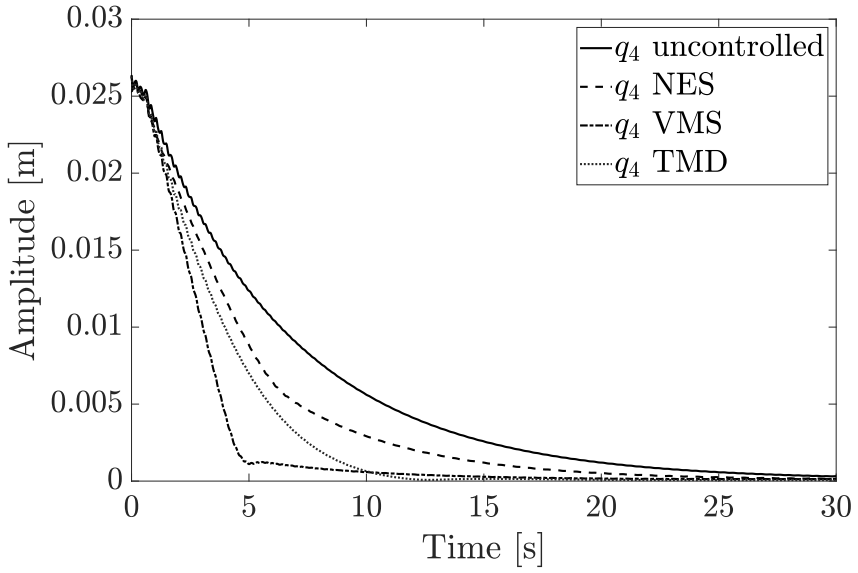

Figure 10: The 4 DOF building: positive envelopes of the impulse response for q_4 for different absorbers.

Table 2: 2%-settling times [s] of the top floor q_4 for the 4 DOF building

	original system	VMS ($N_1 = 1.6635$)	VMS ($N_1 = 5.9467$)	TMD	NES
q_4	24.25	11.81	10.01	14.54	22.88

specifically by adjusting its mass with ±10% and changing the damping accordingly to keep the damping ratio at 1%. The resulting 2%-settling times are visualised in Figure 11a. To take into account the effect of the shifting eigenfrequencies due to changing mass on the settling time, the amount of fundamental periods κ until the 98% amplitude decrease of the top floor is reached, is plotted on the y-axis and the relative change in mass on the x-axis.

The VMS controllers are performing the best around zero mass change, but when the mass is changed more drastically, the settling time increases. This can be expected as the VMS is made sensitive to a specific frequency. This is the case for the TMD as well. From ±1.5% mass change the performance of the VMS is even slightly worse than for the TMD, but they tend to keep a similar trend throughout the mass variation. This means that the TMD is also able to create sufficient energy transfer from the top floor to the

bottom floor. The NES does barely better than the uncontrolled situation and the mass variation has only a limited effect on its performance. This poor result for the NES can be explained by its location. The energy in the bottom floor is the lowest for the first vibration mode, so the activation energy threshold is almost not reached, resulting in a large amount of residual energy.

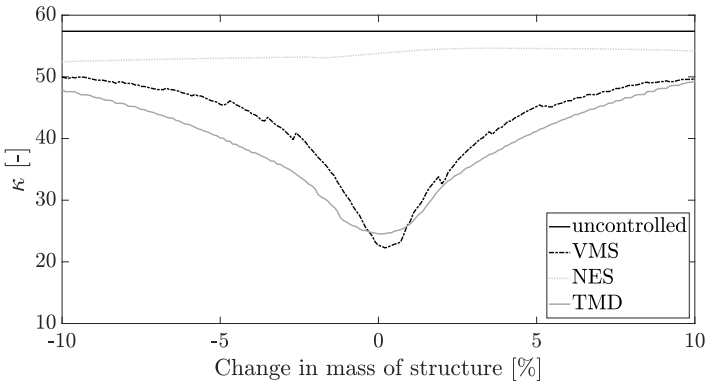

(a)

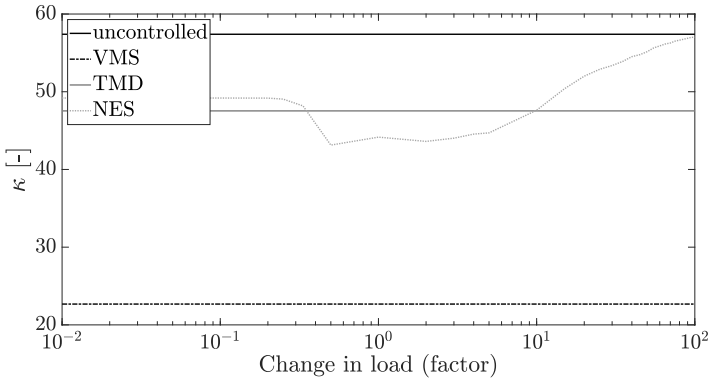

(b)

Figure 11: Robustness of the controllers for the 4 DOF case. (a) Number of fundamental periods until 98% energy dissipated for different vibration control strategies with model errors. (b) Comparison of performance of different vibration control strategies for different magnitudes of the load.

The influence of the load is also investigated and the results are depicted in Figure 11b. One can observe that the performance of the NES is susceptible to changes in the magnitude of the load, which is expected. From an initial velocity of $\dot{q}_4 = 2 \cdot 10^{-1} m/s$

the settling time improves slightly, but from $\dot{q}_4 = 2 \cdot 10^1 m/s$ the performance worsens rapidly, until it even gets equally worse than the uncontrolled system at $\dot{q}_4 = 10^2 m/s$. In contrast, the TMD and VMS demonstrate consistent settling times. They are unaffected by the size of the force. This advantage of the TMD compared to the NES is also present in the VMS controller.

4. Examples - 60 DOF building

In the 4 DOF building example, the TMD and VMS are able to transfer the energy from the top floor to the lowest floor. In this example the energy transfer path's length is increased significantly to investigate whether this effect remains valid for a 60 DOF building. Let us consider the case where an impulse load, that introduces vibrations, is applied at q_{60}, while the VMS controller is attached at q_1, again the furthest from the energy source. This load is equivalent to setting the initial condition $\dot{q}_{60} = 1 m/s$, while all other velocities are 0. First, the tuning methodology of Section 2.1.3 with the VMS will be applied to the 60 DOF building. Next, a TMD and NES are tuned for this system, as they represent the state-of-the-art in (passive) vibration control of buildings.

The model is found in [26], which is a benchmark system. The matrices of (1) are given by

$$M = 1\ 200\ 000 \cdot I_{60} \quad [kg] \tag{38}$$

$$K = \begin{bmatrix} 2k & -k & 0 & \dots & 0 & 0 \\ -k & 2k & -k & \dots & \vdots & \vdots \\ 0 & -k & 2k & \dots & 0 & 0 \\ \vdots & \vdots & \vdots & \ddots & -k & 0 \\ 0 & \dots & 0 & -k & 2k & -k \\ 0 & \dots & 0 & 0 & -k & k \end{bmatrix}, \text{with } k = 2\ 200\ 000\ 000 \quad \left[\frac{N}{m}\right] \tag{39}$$

A damping ratio of $\zeta = 0.5\%$ is assumed. This allows to calculate $C = E^{-T} 2 Z \Omega E^{-1}$, with E the mass-normalised eigenvectors, $Z = \zeta \cdot I_{60}$, and $\Omega = diag(\omega_i)$. The five lowest (most dominant) eigenfrequencies can be found in Table 3.

From the impulse response of the 60^{th} floor, it can be seen that the first eigenfrequency dominates, so only this mode is considered in the remainder of the analysis.

Table 3: First five eigenfrequencies [rad/s] of the 60 DOF building.

ω_1	ω_2	ω_3	ω_4	ω_5
1.1117	3.3342	5.5546	7.7712	9.9825

4.1. Virtual mechanical system and modal system approximation

As we only consider the first mode of the structure to design the controller (see above), the dimension of the controller will be $n_c = 1$. Hence, the controller structure is similar to the example of the 4 DOF building with $\mathbf{N} = \begin{bmatrix} N_1 & 0 & \dots & 0 & 0 \end{bmatrix} \in \mathbb{R}^{60}$. The virtual stiffness is $K_0 = \omega_1^2$, as in (24), and from (25) $N_1 = 1289.9730$ is found. This choice for N_1 succeeds in placing the new pole pair, which is introduced by adding the VMS controller to the system, close to the dominant pole pair of the main system (see Figure 12a). Hence, one can confirm that this method remains valid for large structures.

From Figure 12b it can be seen that beating occurs between the top floor and the controller's coordinate, even though the movement of floor one q_1 is very small. The controller manages to attract just about all energy from q_{60} to z. The energy transfer of the first mode is maximal around 370s. Parameter N_1 could be further optimised as placing the poles in the real system further apart leads to a faster beating frequency, but there is a trade-off. The minimal amount of energy that remains in the top floor is increasing as well. This is depicted in Figure 13. However, no further optimisation is done at this point, it is just meant to demonstrate the presence of a trade-off.

4.2. Nonlinear damping

The same damping function (34) is used in the 60 DOF case. This leads to a 2%-settling time of the top floor of 343.0336s, which is a decrease of 51.16%. With the damping in place, N_1 can be further optimised. An optimisation is performed to minimise the settling time of q_{60}. Notice that the internal damping of the function is rather low and does not aid the mitigation of vibrations as much as in the 4 DOF case. For this reason, the percentual change of N_1 is limited and there is less design freedom. The optimisation leads to $N_{1,opt} = 1.38 \cdot N_1 = 1780.1628$. The resulting envelopes of the time responses of the top floor can be found in Figure 14. The performance of the VMS controller, both with N_1 and $N_{1,opt}$ is compared to the original system. The 2%-settling

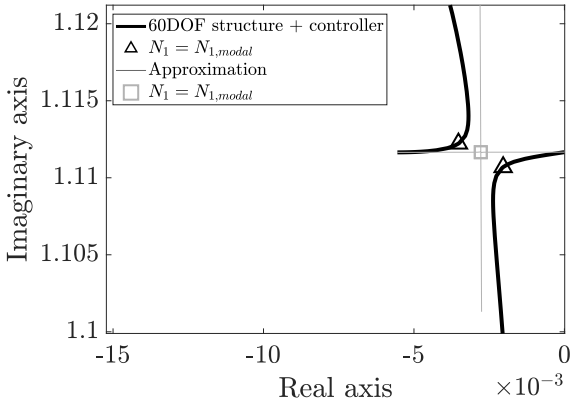

(a)

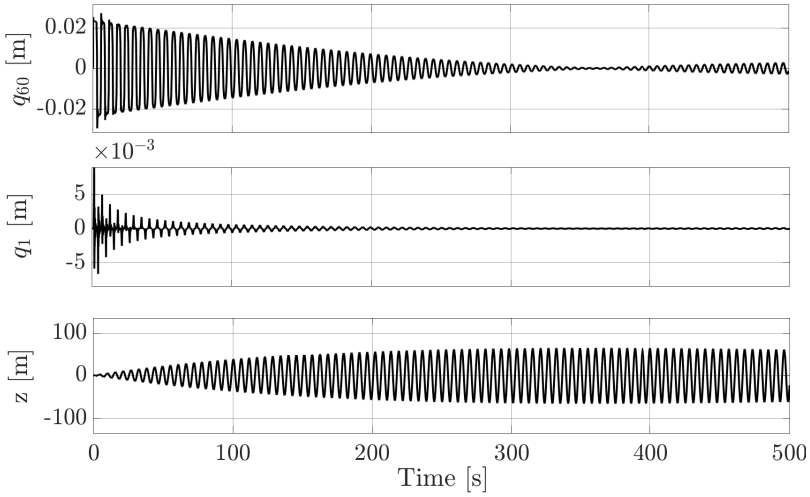

(b)

Figure 12: (a) Comparison of dominant poles with varying N_1 for the original 60 DOF system and the modal approximation. (b) Impulse response of top and bottom floor and the controller coordinate for the controlled 60 DOF system. There is no damping present in the controller.

times for these cases are 343.0336s, 288.6971s, and 702.4131s respectively. The optimised controller achieves a reduction of 58.90%.

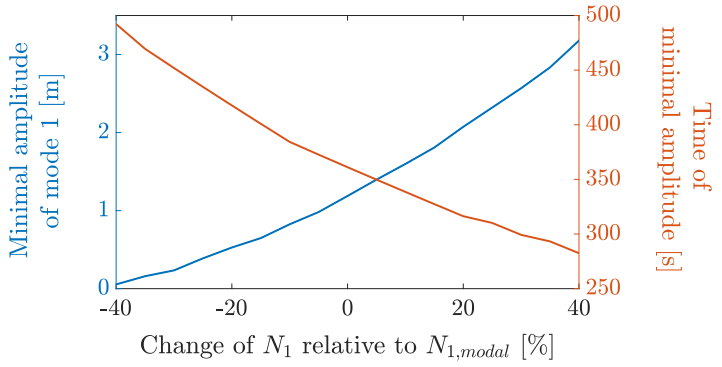

Figure 13: Trade-off between speed and amount of energy transfer for the 60 DOF system in function of N_1.

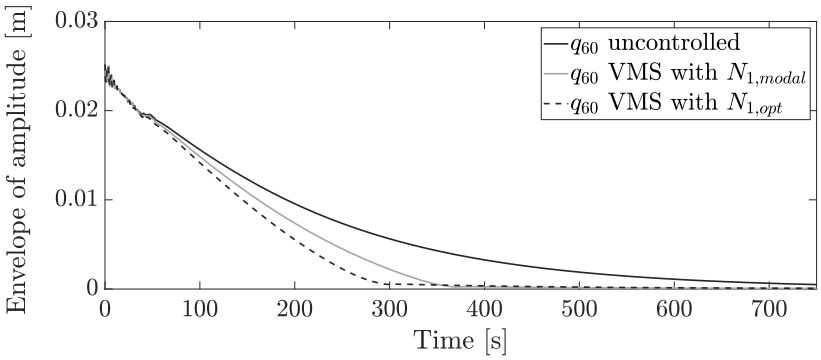

Figure 14: Impulse responses of the top floor for the original 60 DOF system and the systems with the VMS controllers.

4.3. TMD/NES

The same tuning methodology is used as in the 4 DOF case. We refer to Section 3.4 for an in depth explanation on the tuning and design choices. The numerical values of the parameters are given in Table 4.

Table 4: Parameters of the TMD/NES for the 60 DOF building.

$m_a[kg]$	$c_a[Ns/m]$	$k_a[N/m]$	$c_{na}[Ns/m]$	$k_{na}[N/m]$
$3.60 \cdot 10^5$	$2.07 \cdot 10^3$	$4.45 \cdot 10^5$	$5.00 \cdot 10^4$	$1.53 \cdot 10^{11}$

The 2%-settling times of each of the vibration mitigation methods discussed can be

found in Table 5. Notice that the VMS controllers are again able to decrease the settling time significantly. For the NES the same observation can be made as in the 4 DOF case. The NES does not result in a relevant improvement, due to the lack of energy it observes at the lowest floor. The TMD is not able to obtain the same improvement as the VMS controller. However, the TMD is still able to reduce the settling time significantly compared to the uncontrolled/NES case.

Table 5: 2%-settling times [s] of the top floor q_{60} for the 60 DOF building

	original system	VMS ($N_1 = 1289.9730$)	VMS ($N_1 = 1780.1628$)	TMD	NES
q_4	702.41	343.03	288.70	561.13	702.41

4.4. Robustness

The same methodology as in the 4 DOF case has been used. Figure 15 represents the robustness to model errors. The floors' mass has been changed by $\pm 10\%$, thus, altering the eigenfrequencies of the structure. Again, the effect of matching the eigenfrequencies is very important for the VMS controllers, as for the TMD. When this property is not fulfilled, the controllers' performance drop. The VMS is very capable of transferring the energy of the top floor to the bottom floor using this beating phenomenon. The TMD is also capable to transfer some energy, but not as effectively, as opposed to the 4 DOF building example. The TMD struggles with a longer energy transfer path. The NES is not able to improve the settling time of the building compared to the uncontrolled case. This is for the same reason as in the 4 DOF building example: there is not enough energy of the first vibration mode present in the first floor, due to the long transfer path from the impact location (top floor) to the controller location (bottom floor).

5. Discussion

5.1. Interpretation of control policy

The control strategy proposed in this paper proves its merits for vibration mitigation in building structures. The key lies in capturing the dominant mode of the main system.

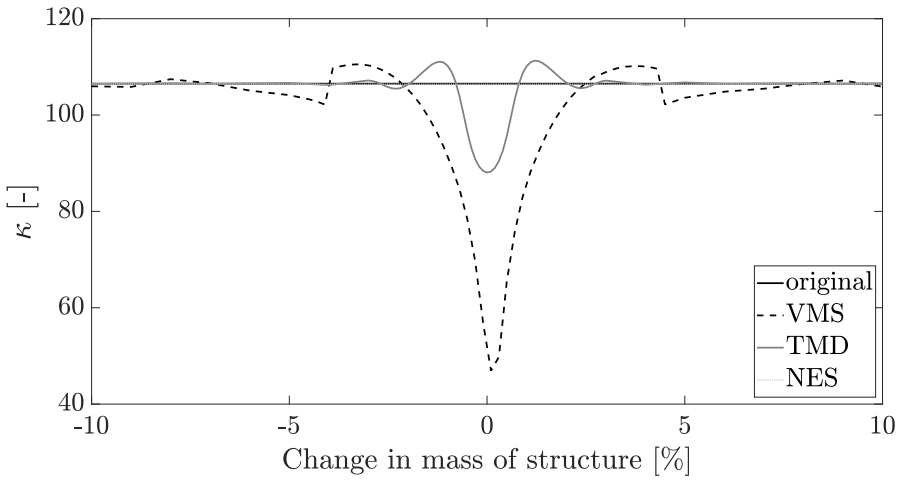

Figure 15: Number of fundamental periods until 98% energy dissipated for different vibration control strategies with model errors for the 60 DOF case study.

Due to the addition of the VMS controller, and especially due to the unique coupling between the VMS and the main system, a new mode, where only z vibrates, is imposed on the system. Because of the choice of the coupling term N_1, this new mode has an eigenfrequency close to that of the dominant mode of the main system. Hence, the energy of the latter mode can be attracted to the VMS by exploiting the beating phenomenon, even though only one generalised coordinate is actuated.

5.2. Controller parameters

In order to create the desired behaviour, K_0 is chosen to match the eigenfrequency of the VMS to that of the main system (see (24)), analogous to a TMD. The coupling terms ν and N, are chosen as $\nu = -N^T$ to guarantee stability, and as such form a skew-symmetric interconnection matrix. This means gyroscopic forces are introduced in the controlled system. By varying N, the position of the poles in the complex plane can be influenced. By applying (25), the two dominant pole pairs of the controlled system lie close together. As their eigenfrequencies only differ slightly, a beating phenomenon arises between the generalised coordinates of the main system and the virtual coordinate. One can furthermore choose to optimise the value of N depending on the application. The optimisation criterion in this work is the 2%-settling time of the generalised coordinates

of the main system. In case an optimisation is executed, (25) offers a good starting point. The two pole pairs and the N region that needs to be explored are known, which substantially simplifies the optimisation process.

The further the pole pairs are separated, the higher the beating frequency, to some extent (see (27)). The trade-off here lies in the fact that a higher beating frequency leads to faster energy transfer, however it has a technical drawback. The switching time of the damping t_{switch} in (34) is estimated based on the envelope of the time response, which is calculated online. A beating signal contains two frequencies: first, the beat frequency (27), which is a periodic amplitude modulation, and, second, the higher vibrational frequency

$$f_v = \frac{f_p + f_c}{2}. \tag{40}$$

The ratio of the vibrational frequency over the beat frequency is a measure of the time resolution for the envelope estimation. The higher the ratio, the more peaks in the fast periodic signal to estimate the slower beat frequency are present. In the case that we assume that $f_c = f_p - \sigma$, with $\sigma \in \mathbb{R}_{>0}$, the ratio is given by:

$$\frac{f_p + f_c}{|f_p - f_c|} = \left| \frac{2f_p}{\sigma} - 1 \right|. \tag{41}$$

This means that if the poles are further separated, that σ increases, which means that the ratio drops for $\sigma \in]0, 2f_p]$. Hence, there are less peaks of the vibrational signal in one period of a beat. This leads to a less accurate estimate of the envelope, and, thus, of the switching time of the damping. However, if enough damping is present in the main system, the energy that is not captured by the VMS can be dissipated by the damping in the main structure (see 4 DOF benchmark, Figures 8a and 8b).

A big merit of this active control strategy, is that the damping force can be chosen freely, within the conditions formulated in the stability proof in Section 2.1.1. This is taken advantage of to allow energy attraction towards the controller, while energy transfer back to the main system is inhibited.

5.3. Comparison to TMD and NES

When comparing the performance of the VMS control strategy to the TMD and NES, following remarks can be made.

In Figure 10, for the 4DOF building, one can see that the NES is able to withdraw energy from the main system initially, but from 5s onwards the decay is mainly due to the internal damping of the main system. The TMD has an exponential decay until the end, and is able to mitigate the vibrations quickly. However, the VMS is able to remove the vibrational energy much faster compared to the passive solutions. For the 60 DOF building, in Figure 14, the NES is still not able to decrease the settling time, and the TMD struggles to capture all the energy present in the building, because of the longer energy transfer path in this case study. After all, this leads to a smaller relative displacement between the additional structure and the controlled floor. The VMS keeps outperforming the passive solutions with a 60% faster settling time compared to the uncontrolled building. Hence, the introduction of the beating phenomenon as a tuning strategy is robust to longer energy transfer paths. The NES initially gets more energy out of the system than the TMD, as its nonlinear stiffness allows it to capture multiple frequencies, as is visible in Figure 9. The underperformance of the passive devices can also be contributed to the fact that they exert a force that depends on the relative displacement between q_1 and the absorber. This offers a challenge as q_1 has the smallest amplitude when the load is applied to the top floor q_n, and the first vibrational mode is dominant.

From the robustness studies in Figure 11a and 15 for the 4 DOF and 60 DOF building respectively, it is clear that the VMS and TMD are tuned to a specific frequency. The efficacy diminishes significantly if the mass of the building's floors is changed, which leads to a shift of the buildings first eigenfrequency. The NES is almost insensitive to this change in eigenfrequency, but is affected by the size of the impact force. Further one can note that the VMS shows its merits more profoundly compared to the TMD in the 60 DOF case, while 4 DOF case this is less pronounced. However, in the 60 DOF building case, from 2% mass change the TMD, NES and VMS perform equally bad, but it should be noted that the VMS is an active controller. Hence, updating the eigenfrequency of the virtual system is merely an adaption of the programmed values, opposed to the passive solutions, where a new mechanical design is necessary.

6. Conclusion

In this study, an active control policy is proposed, inspired by passive vibration absorbers, but with more freedom in the coupling of the systems. The stability of the controlled system is investigated using Lyapunov's direct method. Considering the stability conditions and a modal approximation of the main system, a tuning method for the controller parameters is put forward. Furthermore, in a 4 DOF and 60 DOF benchmark the performance is investigated with respect to the TMD and NES. Here, the VMS succeeded in decreasing the settling time with approximately 60% in both cases. The TMD achieved a reduction of 40% in the 4 DOF case and of 20% in the 60 DOF case. The NES did not improve the settling time for both benchmarks, due to the fact that the energy of the first vibrational mode at its attachment location is too low. The TMD struggles with a longer energy transfer path, while the VMS is more capable of dealing with taller structures, and thus a longer energy transfer path.

This strategy, based on a VMS, effectively mitigates vibrations in n DOF structures. The key to the success of this approach lies in the specific tuning of the parameters, which causes a beating phenomenon to arise. This is a consequence of the unique coupling between the VMS and the main structure. Taking advantage of this beating phenomenon, the energy is effectively attracted to the VMS, while only actuating at one coordinate, which is moreover the furthest from the source. Finally, the freedom provided by the use of a VMS allows for nonlinear damping for targeted energy dissipation. A damping is proposed based on the (estimate of) the envelope of the virtual coordinate, which is switched on once the maximum is reached. It is shown that a relatively bad estimate of this switching time still results in a good performance.

This research has contributed new knowledge to the field by, first, providing a set of stable active controllers that allow for intuitive tuning and, second, proposing a tuning method that effectively causes energy to be attracted from all generalised coordinates to the point where it can be dissipated.

References

[1] Z. A. B. Ahmad, K. H. Hui, M. H. Lim, M. S. Leong, Building floor vibration due to in-building speed bump, Journal of Performance of Constructed Facilities 32 (4) (2018).

[2] W. B. Bao, Y. Y. Hu, Y. Cui, Wind loads simulation of tall building structures subjected to wind-structure interaction, Advanced Materials Research 163–167 (2010) 4286–4289.

[3] F. Yoshiyuki, T. Izuru, Critical earthquake input energy to connected structures using impulse input, Earthquakes and Structures 9 (6) (2015) 1133–1152.

[4] C. R. Ashokkumar, Vibration control for structural damage mitigation, Journal of Vibration and Control 21 (15) (2015) 2995–3006.

[5] M. Sheehan, Everyday verticality: Migrant experiences of high-rise living in santiago, chile, Urban Studies (2022).

[6] T. Kalaycioglu, H. N. Ozguven, Harmonic response of large engineering structures with nonlinear modifications, in: G. DeRoeck, G. Degrande, G. Lombaert, G. Muller (Eds.), Proceedings of the 8th International Conference on Structural Dynamics, EURODYN 2011, 2011, pp. 3623–3629.

[7] D. T. R. Pasala, A. A. Sarlis, S. Nagarajaiah, A. M. Reinhorn, M. C. Constantinou, D. Taylor, Adaptive negative stiffness: New structural modification approach for seismic protection, Journal of Structural Engineering 139 (7) (2013) 1112–1123.

[8] M. Sen, O. Cakar, A new method for reducing the number of resonance frequencies of mechanical systems within a specified frequency range with inverse structural modification and pole-zero cancellation, Journal of Vibration and Control (2023). doi:10.1177/10775463231205353.

[9] A. Paknejad, G. Zhao, S. Chesné, A. Deraemaeker, C. Collette, Design and optimization of a novel resonant control law using force feedback for vibration mitigation, Structural Control and Health Monitoring 29 (6) (2022) e2939.

[10] H. Hojat Jalali, M. Fahimi Farzam, S. A. Mousavi Gavgani, G. Bekdaş, Semi-active control of buildings using different control algorithms considering ssi, Journal of Building Engineering 67 (2023) 105956.

[11] S. Elias, V. Matsagar, Research developments in vibration control of structures using passive tuned mass dampers, Annual Reviews in Control 44 (2017) 129–156.

[12] Z. Lu, Z. Wang, Y. Zhou, X. Lu, Nonlinear dissipative devices in structural vibration control: a review, Journal of Sound and Vibration 423 (2018) 18–49.

[13] L. Wang, S. Nagarajaiah, W. Shi, Y. Zhou, Seismic performance improvement of base-isolated structures using a semi-active tuned mass damper, Engineering Structures 271 (2022) 114963.

[14] L. Wang, Y. Zhou, S. Nagarajaiah, W. Shi, Bi-directional semi-active tuned mass damper for torsional asymmetric structural seismic response control, Engineering Structures 294 (2023) 116744.

[15] Chesné, Simon, Hybrid skyhook mass damper, Mechanics & Industry 22 (2021) 49.

[16] L. Koutsoloukas, N. Nikitas, P. Aristidou, Passive, semi-active, active and hybrid mass dampers: A literature review with associated applications on building-like structures, Developments in the Built Environment 12 (2022) 100094.

[17] M. H. El Ouni, M. Abdeddaim, S. Elias, N. B. Kahla, Review of vibration control strategies of high-rise buildings, Sensors 22 (21) (2022) 8581.

[18] J. Juchem, M. Loccufier, Vibration control of underactuated mechanical systems with non-linear euler-lagrange control, in: Proceedings of the European Control Conference 2023, ECC23, 2023,

pp. 282–287.

[19] M. L. Adams, M. Rashidi, On the use of rotor-bearing instability threshold to accurately measure bearing rotordynamic properties, Journal of Vibration, Accoustics, Stress, and Reliability in Design 107 (1985) 404–409.

[20] J. Yuan, S. Fei, Y. Chen, Technical note: On the actuator rate limit effect in reaction curves, ISA Transactions 117 (2021) 303–308.

[21] B. G. Korenev, L. M. Reznikov, Dynamic vibration absorbers: theory and technical applications, Wiley, 1993.

[22] T. Asami, O. Nishihara, A. M. Baz, Analytical Solutions to H_∞ and H_2 Optimization of Dynamic Vibration Absorbers Attached to Damped Linear Systems , Journal of Vibration and Acoustics 124 (2) (2002) 284–295.

[23] K. Dekemele, R. De Keyser, M. Loccufier, Performance measures for targeted energy transfer and resonance capture cascading in nonlinear energy sinks, Nonlinear Dynamics 93 (2018) 259–284.

[24] K. Dekemele, G. Habib, Inverted resonance capture cascade: modal interactions of a nonlinear energy sink with softening stiffness, Nonlinear Dynamics (2023) 1–23.

[25] K. Dekemele, Performance measures for nonlinear energy sinks in mitigating single and multi-mode vibrations: theory, simulation and implementation, Ph.D. thesis, Ghent University (2021).

[26] K. S. Moon, Vertically distributed multiple tuned mass dampers in tall buildings: performance analysis and preliminary design, The Structural Design of Tall and Special Buildings 19 (3) (2010) 347–366.